

COMMUNICATION

The Structure of a Filamentous Bacteriophage

Ying A. Wang¹, Xiong Yu¹, Stacy Overman², Masamichi Tsuboi²
George J. Thomas Jr^{2*} and Edward H. Egelman^{1*}

¹Department of Biochemistry
and Molecular Genetics
University of Virginia
Box 800733, Charlottesville
VA 22908-0733, USA

²School of Biological Sciences
University of Missouri-Kansas
City, 5100 Rockhill Road
Kansas City, MO 64110-2499
USA

Many thin helical polymers, including bacterial pili and filamentous bacteriophage, have been seen as refractory to high-resolution studies by electron microscopy. Studies of the quaternary structure of such filaments have depended upon techniques such as modeling or X-ray fiber diffraction, given that direct visualization of the subunit organization has not been possible. We report the first image reconstruction of a filamentous virus, bacteriophage fd, by cryoelectron microscopy. Although these thin (~70 Å in diameter) rather featureless filaments scatter weakly, we have been able to achieve a nominal resolution of ~8 Å using an iterative helical reconstruction procedure. We show that two different conformations of the virus exist, and that in both states the subunits are packed differently than in conflicting models previously proposed on the basis of X-ray fiber diffraction or solid-state NMR studies. A significant fraction of the population of wild-type fd is either disordered or in multiple conformational states, while in the presence of the Y21M mutation, this heterogeneity is greatly reduced, consistent with previous observations. These results show that new computational approaches to helical reconstruction can greatly extend the ability to visualize heterogeneous protein polymers at a reasonably high resolution.

© 2006 Elsevier Ltd. All rights reserved.

*Corresponding authors

Keywords: polymorphisms; helical polymers; cryo-EM

Filamentous bacteriophages have been investigated extensively using biophysical and molecular biological techniques. Class I (Ff strains fd, f1 and M13) and class II (Pf1), virions have been exploited for purposes as diverse as cloning, antigen display and small molecule alignment.¹ Phage fd has been the class I strain of choice for structural studies.^{2–4} The fd particle (~7 nm × 880 nm) consists of a covalently closed, single-stranded DNA genome (6408 nucleotides) sheathed by 2750 copies of a 50 residue α -helical subunit (pVIII) plus a few copies of minor proteins at the filament ends. In oriented fibers⁵ of the mature phage, the pVIII α -helix axis is tilted from the virion axis by an angle of 16(±4)°. Although structural models of fd have been generated by X-ray fiber diffraction,^{3,6} and by solid-state NMR,⁴ they disagree fundamentally in

the orientation and continuity of the subunit α -helix.

We have used electron microscopy to re-examine fd structure. The negatively stained particle (Figure 1(a)) is visualized as a featureless, flexible rod. Using such images to calculate the equilibrium persistence length of fd, which is a measure of flexural rigidity, we obtain 1.0 μ m (Figure 1(b)), a factor of 2 lower than reported previously.⁷ This helps resolve a discrepancy, inasmuch as the dynamic persistence length⁸ was reported as 2.2 μ m and studies of other systems indicated an equilibrium persistence length significantly smaller than the dynamic value.⁹ Cryoelectron microscopy micrographs of fd filaments (Figure 1(c)) also appear featureless, but actually contain high-resolution information compromised by a poor signal-to-noise ratio.

The first 3D electron microscopy reconstruction was obtained from a helical tail assembly of bacteriophage T4 using Fourier–Bessel analysis.¹⁰ The Fourier–Bessel methods are limited in the reconstruction of thin and relatively featureless filaments, owing to dependence upon a signal-to-

Abbreviation used: IHRSR, iterative helical real space reconstruction.

E-mail addresses of the corresponding authors:
thomasgj@umkc.edu; egelman@virginia.edu

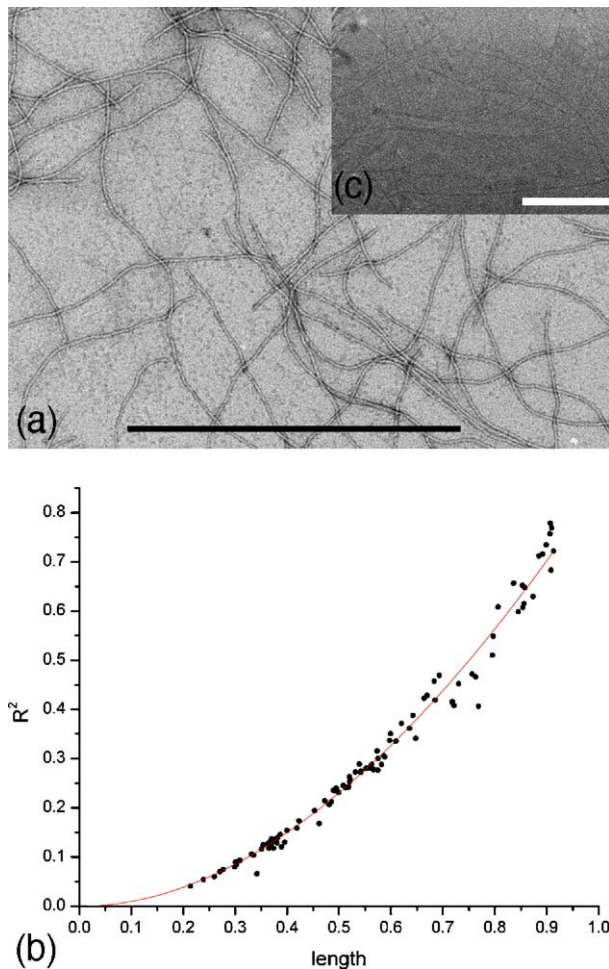


Figure 1. Electron micrographs of negatively stained fd (a) used to obtain the persistence length P by fitting the contour length L between two points as a function of the square of their separation, R^2 , (b) according to the relationship:²⁸ $R^2 = 4PL [1 - (2P/L)(1 - \exp(-L/2P))]$. The best fit (red line) yields $P = 1.02(\pm 0.06)$ μm , where the error was determined by the non-linear curve-fitting algorithm in the program Origin 7.5 (OriginLab Corporation). From prior results using both real data and simulations,²⁹ we expect that this is an underestimate of the true error, but expect the error to be less than 0.5 μm . (c) Images in ice (inset) were collected on a Tecnai 20 field emission gun microscope at 200 keV. The 23 \AA pitch helix of TMV was used to determine the magnification. Defocus values of 1.4–3.8 μm from 67 micrographs of wild-type fd were determined from the carbon film supporting the phage or adjoining holes in which the phages were imaged. The contrast transfer function was corrected by phase-flipping before subsequent image processing. The space bar represents (a) 0.9 μm and (c) 0.4 μm .

noise ratio sufficiently large that layer-lines may be extracted from single particles. Additionally, because uniform symmetry and structure are imposed on the targeted filament, heterogeneous regions may be averaged.¹¹ We have used the iterative helical real space reconstruction (IHRSR) method to reconstruct fd.¹² Data were obtained from native specimens prepared under conditions that

minimize aggregation.¹³ Using 84,310 filament segments (each of length 240 \AA) extracted from filaments in ice, we failed to achieve convergence to a common structure from different starting symmetries. This suggested structural polymorphism. By using two different initial reconstructions and employing multiple iterations of the algorithm, we were able to classify the segments into three groups, two of which ($n_1 = 25,440$, $n_2 = 16,367$) generated reconstructions that converged independent of the starting symmetry (Figure 2). The third group ($n_3 = 42,503$) failed to converge, and we were unable to sort this group into more homogeneous subsets. The reconstructions generated from n_1 and n_2 are shown in Figure 3(a) and (b), respectively, and it can be seen that they are different. We determined the resolution of these reconstructions to be ~ 8 \AA (Figure 3(g)). While the symmetry of these two structures is nearly indistinguishable, they differ structurally, and these structural differences explain why the IHRSR method did not achieve convergence using the whole population of images. The two reconstructions have a Fourier shell correlation (FSC) of 0.5 at a resolution of 1/(14 \AA). This does not mean that the two reconstructions are indistinguishable at 14 \AA resolution, but rather that within this resolution shell the two have a correlation of only 0.5.

We have excluded the possibility that the two different structural states are an artifact arising from different defocus values or some other aspect of the microscopy, as the two states are found on the same micrographs. Further, we have observed that the two different states can be found in the same phage particle, excluding the possibility that an entire phage is entirely in one state or the other. As with all structures generated from EM images, there is an enantiomorphic ambiguity in our reconstructions. That is, each reconstruction can be mirrored to generate a second reconstruction, and both enantiomorphs will produce the same set of projections. We have excluded the possibility that the two structures are simply enantiomorphs of each other. Because of the symmetry of the phage, there is a rotation of $36.0 + \delta^\circ$ from one subunit to a subunit 17.4 \AA above it, and this can be expressed as a rotation of $-36.0 - \delta^\circ$. That is, $+34.6^\circ$ is the same as -37.4° . Because of the enantiomorphic ambiguity, a reconstruction with a symmetry involving a $+34.6^\circ$ (or -37.4°) rotation cannot be distinguished with our data from the mirror image of this reconstruction, which will have a rotation of -34.6° (or $+37.4^\circ$). We have relied upon the X-ray diffraction data,² which suggested that the subunits are slewed in a right-handed manner, to choose the enantiomorphs shown, which correspond to a rotation of $\sim 37.4^\circ$ between a subunit and the one above it.

Numerous studies have suggested that the subunit is quite malleable,^{1,14} which is consistent with the capsid polymorphism evident here. In fact, a minimized fd (M13) coat protein in which all but nine of the 50 residues were mutated to Ala was found to co-assemble efficiently with the wild-type protein to produce infectious particles.¹⁵ Because conformational heterogeneity of wild-type fd was

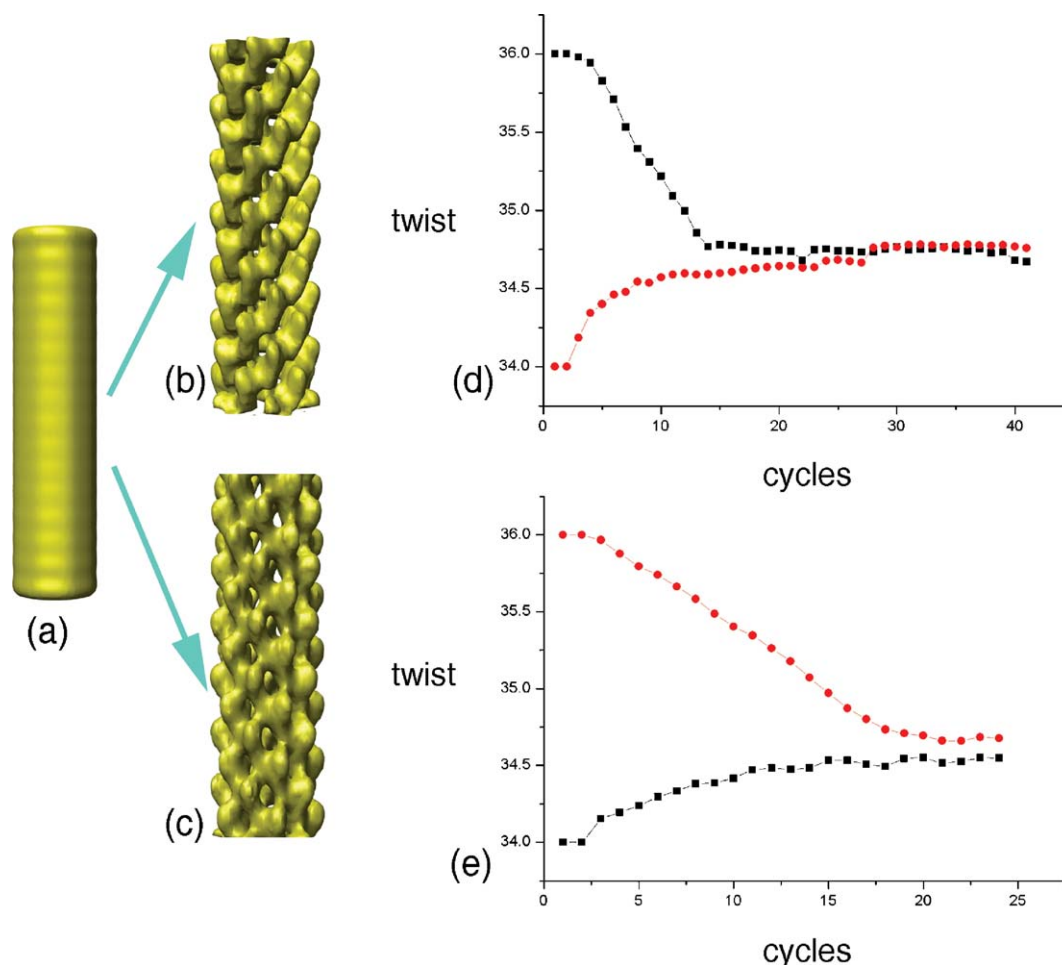


Figure 2. The failure of the IHRSR method to converge to a single structure and symmetry from different initial values is indicative of heterogeneity. (a) Reconstructions were initiated using a solid cylinder as a starting model with different starting symmetries. (b) and (c) The resulting reconstructions are different. By using the two different initial reconstructions and employing multiple iterations of the algorithm, we were able to classify the segments into three groups, two of which ((d) and (e)) show convergence independent of the starting symmetry. The axial rise per subunit is also free to change in the IHRSR approach and, using initial values of 15.8 Å and 17.4 Å, we have always seen convergence to 17.4 Å. One group ((d), $n_1=25,440$) generates the reconstruction shown in Figure 3(a), while the second group ((e), $n_2=16,367$) generates the reconstruction shown in Figure 3(b), which is significantly different from that in Figure 3(a).

reported to be reduced in the Y21M mutant, we also examined the mutant.^{3,4} (The mutation occurs in a region of the subunit that putatively links amphipathic and hydrophobic α -helices.) We found that all segments sampled from Y21M could be sorted

roughly equally into the same two (Figure 3(d) and (e)) relatively homogeneous groups ($n_1 \approx n_2 \approx 10,000$) observed for wild-type fd, but with no major heterogeneous population ($n_3 \approx 0$). The somewhat lower resolution (~ 9 Å) achieved for the Y21M

Figure 3. (a) and (b) Surfaces from two different reconstructions of wild-type fd. The subunit N terminus is toward the top and on the phage exterior. In (b), several subunits are numbered to illustrate the 5-fold rotational symmetry of the structure (e.g. subunits i and $i+6$ are related by a 37.4° rotation and 17.4 Å axial rise). An α -helical subunit was built into the reconstruction by starting with the X-ray model **1IFD** and allowing additional bends between residues 15 and 16, 25 and 26, and 35 and 36. The α -helix shown includes residues 6–48. Residues 1–5 have been described as disordered and are presumed to correspond to the small additional density that is unaccounted for by the atomic model (red arrow). (c) A cutaway view of the lumen, obtained by removing the front half of the reconstruction, where subunit C-terminal ends form a right-handed five-start helical groove. The coordinates of our model are available from the Protein Data Bank. (d) and (e) The corresponding reconstructions from the Y21M mutant. (f) The comparison of different subunit models shows our fit (b, green), the most recently refined X-ray model (**2C0W**, red) and the NMR model (**1NH4**, cyan). The two views shown are related by a 90° rotation about the helical axis (black). The IHRSR method also allows for the estimation of resolution by comparing truly independent reconstructions, each containing the entire data set, but generated from different starting points,^{30–32} and (g) a value of ~ 8 Å was found by this approach for the reconstruction shown in (a). Using the more conventional approach of dividing a data set into halves after alignment to a common reference, a similar value of ~ 8 Å was also found. Nearly identical Fourier shell correlation (FSC) curves were obtained for the reconstruction in (b), showing that the difference between the two states is not due to any difference in resolution.

reconstructions is attributed to the smaller number of segments sampled.

A single continuous α -helical subunit does not satisfactorily fit into the reconstruction of that in Figure 3(a), consistent with suggested discontinuity in the α -helix.⁴ In contrast, a continuous α -helix (residues 6–48) flanked by terminal residues (1–5, 49 and 50) in unspecified conformations readily fits the Figure 3(b) reconstruction in accord with reported disorder of the N terminus.⁴ The Figure 3(b) model

is consistent also with the experimental observation that Tyr 21 and Tyr 24 are buried at a hydrophobic intersubunit interface.¹⁶ Although atomic details of the capsid subunit are not resolved, experimentally determined constraints for side-chains, including the orientations of Tyr 21, Tyr 24 and Trp 26,¹⁷ are available for future testing of higher resolution reconstructions. The present results provide a novel view of polymorphism in the native state of the fd virion.

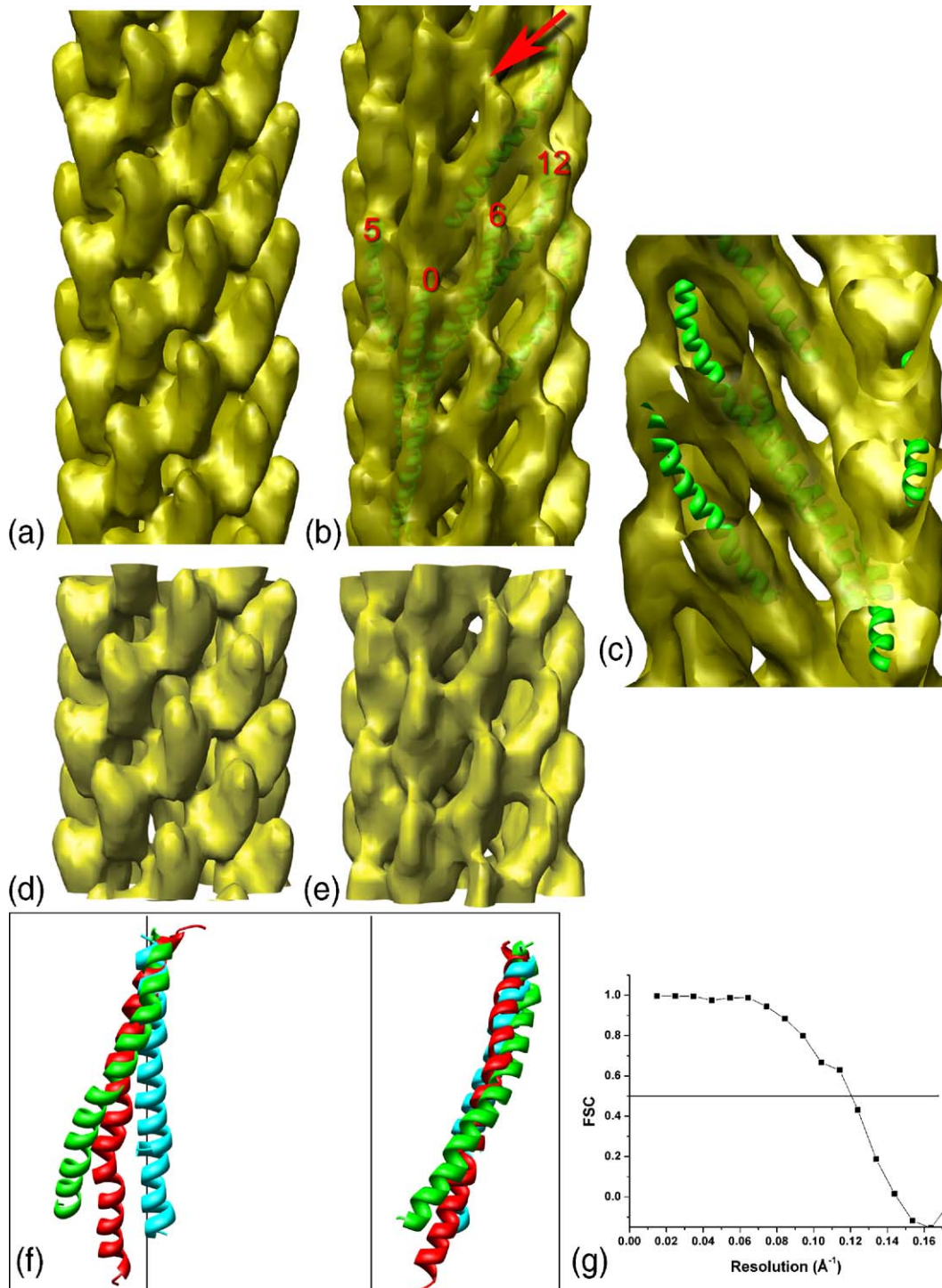


Figure 3 (legend on previous page)

We observe an axial rise per subunit of 17.4 Å in cryoelectron microscopy images of fully hydrated fd (using the 23 Å pitch helix of tobacco mosaic virus (TMV) as a magnification standard). Previous X-ray diffraction studies of dried fibers reported a rise of 16.0 Å.⁶ The shrinkage in fibers used for diffraction is consistent with observations that both the axial rise and the interfilament spacing change as a function of relative humidity in fd and in other filamentous phages.^{18–21}

Figure 3(f) compares the capsid subunit structures proposed on the basis of X-ray fiber diffraction (red, PDB code 2C0W)³ and NMR (cyan, PDB code

1NH4)⁴ with our continuous α -helix model (green). Neither the 2C0W nor the 1NH4 model fits into either reconstruction (Figure 4). Since both the NMR and X-ray fiber diffraction models were based upon the Y21M mutant, it does not seem possible that those two models might fit the data from the wild-type fd that we failed to analyze due to apparent heterogeneity (all of the Y21M segments were classified into one of the two structural states shown in Figure 3(d) and (e)).

The average subunit α -helix tilt angle (θ_h) in our model (Figure 3(b)) is 21°, which is close to the range ($\theta_h=16\pm 4$) found in oriented fibers.⁵ The small

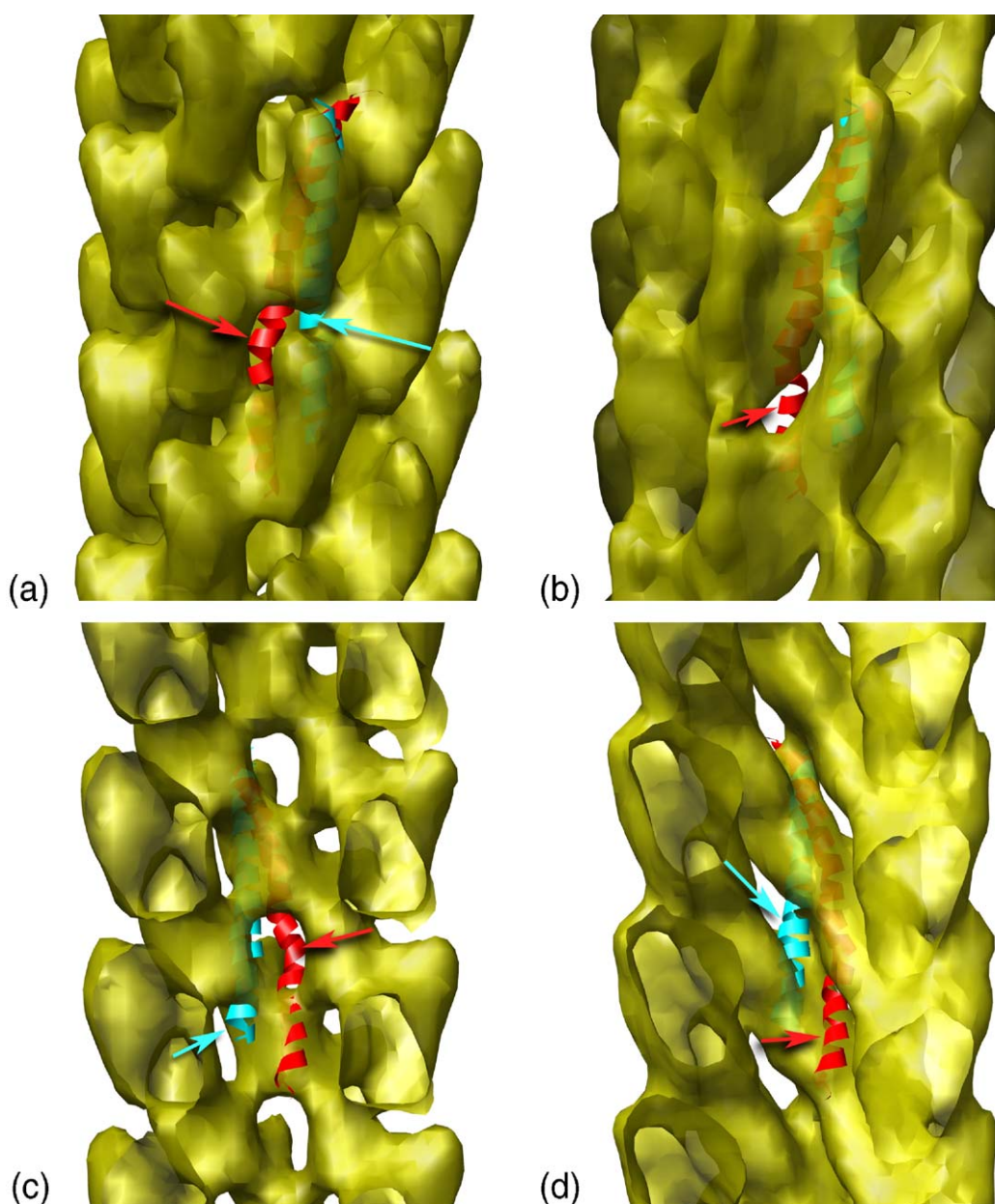


Figure 4. Cryoelectron microscopy reconstructions of the discontinuous α -helix structure shown in Figure 3(a) viewed from (a) the exterior surface and (c) the lumen, illustrating the inability of atomic models from X-ray fiber diffraction (2C0W, red)³ and NMR spectroscopy (1NH4, cyan)⁴ to fit the density distribution accurately. (b) and (d) Corresponding views for the continuous α -helix reconstruction the discontinuous α -helix structure shown in Figure 3(b). Arrows indicate where the existing models are not contained within the density envelope.

difference in average helix tilt may be due to effects of filament aggregation and dehydration in the fibers. While there are not enough constraints to determine an atomic model for the subunit uniquely, given the resolution of the reconstruction, we think that it will be a starting point for refining the structure as well as understanding the structural polymorphism that exists.

Our results demonstrate that the thin and very weakly scattering fd helical assembly, which had been regarded as an unsuitable candidate for electron microscopic 3D reconstruction, can indeed be visualized at a moderately high resolution using the IHRSR approach.¹² In spite of the weak scattering, we have been able to visualize directly a structural polymorphism within the fd capsid, showing that there is not a single unique structure for the virion. This is consistent with the growing body of literature suggesting that other helical protein polymers, such as F-actin,^{22,23} RecA-like proteins,^{24–26} and EspA,²⁷ can exist in a multiplicity of conformational states. In the case of fd, intravirion polymorphism may allow for the flexibility required for host infection and extrusion mechanisms.

Data Bank accession number

The coordinates of our model are deposited with the Protein Data Bank with accession number 2HI5.

Acknowledgements

This work was supported by NIH grants GM035269 and EB001567 (to E.H.E.) and GM50776 (to G.J.T.). We thank Drs Daniel Nemecek and James M. Benevides for helpful comments.

References

- Webster, R. E. (1996). Biology of the filamentous bacteriophage. In *Phage Display of Peptides and Proteins* (Kay, B. K., Winter, J. & McCaffery, J., eds), pp. 1–20, Academic Press, London.
- Glucksman, M. J., Bhattacharjee, S. & Makowski, L. (1992). Three-dimensional structure of a cloning vector. X-ray diffraction studies of filamentous bacteriophage M13 at 7 Å resolution. *J. Mol. Biol.* **226**, 455–470.
- Marvin, D. A., Welsh, L. C., Symmons, M. F., Scott, W. R. & Straus, S. K. (2006). Molecular structure of fd (f1, M13) filamentous bacteriophage refined with respect to X-ray fibre diffraction and solid-state NMR data supports specific models of phage assembly at the bacterial membrane. *J. Mol. Biol.* **355**, 294–309.
- Zeri, A. C., Mesleh, M. F., Nevzorov, A. A. & Opella, S. J. (2003). Structure of the coat protein in fd filamentous bacteriophage particles determined by solid-state NMR spectroscopy. *Proc. Natl Acad. Sci. USA*, **100**, 6458–6463.
- Overman, S. A., Tsuboi, M. & Thomas, G. J., Jr. (1996). Subunit orientation in the filamentous virus Ff (fd, f1, M13). *J. Mol. Biol.* **259**, 331–336.
- Marvin, D. A., Hale, R. D., Nave, C. & Helmer-Citterich, M. (1994). Molecular models and structural comparisons of native and mutant class I filamentous bacteriophages Ff (fd, f1, M13), If1 and IKE. *J. Mol. Biol.* **235**, 260–286.
- Maeda, T. & Fujime, S. (1985). Dynamic light scattering study of fd virus. Application of a theory of the light-scattering spectrum of weakly bending filaments. *Macromolecules*, **18**, 2430–2437.
- Song, L., Kim, U. S., Wilcoxon, J. & Schurr, J. M. (1991). Dynamic light scattering from weakly bending rods: estimation of the dynamic bending rigidity of the M13 virus. *Biopolymers*, **31**, 547–567.
- Naimushin, A. N., Fujimoto, B. S. & Schurr, J. M. (2000). Dynamic bending rigidity of a 200-bp DNA in 4 mM ionic strength: a transient polarization grating study. *Biophys. J.* **78**, 1498–1518.
- DeRosier, D. J. & Klug, A. (1968). Reconstruction of three-dimensional structures from electron micrographs. *Nature*, **217**, 130–134.
- Galkin, V. E., Orlova, A., Van Loock, M. S. & Egelman, E. H. (2003). Do the utrophin tandem calponin homology domains bind F-actin in a compact or extended conformation? *J. Mol. Biol.* **331**, 967–972.
- Egelman, E. H. (2000). A robust algorithm for the reconstruction of helical filaments using single-particle methods. *Ultramicroscopy*, **85**, 225–234.
- Overman, S. A., Kristensen, D. M., Bondre, P., Hewitt, B. & Thomas, G. J., Jr. (2004). Effects of virion and salt concentrations on the Raman signatures of filamentous phages fd, Pf1, Pf3, and PH75. *Biochemistry*, **43**, 13129–13136.
- Sidhu, S. S. (2001). Engineering M13 for phage display. *Biomol. Eng.* **18**, 57–63.
- Roth, T. A., Weiss, G. A., Eigenbrot, C. & Sidhu, S. S. (2002). A minimized M13 coat protein defines the requirements for assembly into the bacteriophage particle. *J. Mol. Biol.* **322**, 357–367.
- Arp, Z., Autrey, D., Laane, J., Overman, S. A. & Thomas, G. J., Jr. (2001). Tyrosine Raman signatures of the filamentous virus Ff are diagnostic of non-hydrogen-bonded phenoxyls: demonstration by Raman and infrared spectroscopy of p-cresol vapor. *Biochemistry*, **40**, 2522–2529.
- Tsuboi, M., Ushizawa, K., Nakamura, K., Benevides, J. M., Overman, S. A. & Thomas, G. J., Jr. (2001). Orientations of Tyr 21 and Tyr 24 in the capsid of filamentous virus Ff determined by polarized Raman spectroscopy. *Biochemistry*, **40**, 1238–1247.
- Caspar, D. L. & Makowski, L. (1981). The symmetries of filamentous phage particles. *J. Mol. Biol.* **145**, 611–617.
- Dunker, A. K., Klausner, R. D., Marvin, D. A. & Wiseman, R. L. (1974). Filamentous bacterial viruses. X. X-ray diffraction studies of the R4-protein mutant. *J. Mol. Biol.* **82**, 115–117.
- Marvin, D. A., Wiseman, R. L. & Wachtel, E. J. (1974). Filamentous bacterial viruses. XI. Molecular architecture of the class II (Pf1, Xf) virion. *J. Mol. Biol.* **82**, 121–138.
- Marvin, D. A., Pigram, W. J., Wiseman, R. L., Wachtel, E. J. & Marvin, F. J. (1974). Filamentous bacterial viruses. XII. Molecular architecture of the class I (fd, If1, IKE) virion. *J. Mol. Biol.* **88**, 581–598.
- Egelman, E. H., Francis, N. & DeRosier, D. J. (1982). F-actin is a helix with a random variable twist. *Nature*, **298**, 131–135.
- Schmid, M. F., Sherman, M. B., Matsudaira, P. & Chiu,

- W. (2004). Structure of the acrosomal bundle. *Nature*, **431**, 104–107.
24. VanLoock, M. S., Yu, X., Yang, S., Lai, A. L., Low, C., Campbell, M. J. & Egelman, E. H. (2003). ATP-mediated conformational changes in the RecA filament. *Structure (Camb.)*, **11**, 187–196.
25. Wu, Y., He, Y., Moya, I. A., Qian, X. & Luo, Y. (2004). Crystal structure of archaeal recombinase RADA: a snapshot of its extended conformation. *Mol. Cell*, **15**, 423–435.
26. Conway, A. B., Lynch, T. W., Zhang, Y., Fortin, G. S., Fung, C. W., Symington, L. S. & Rice, P. A. (2004). Crystal structure of a Rad51 filament. *Nature Struct. Mol. Biol.* **11**, 791–796.
27. Wang, Y. A., Yu, X., Yip, C. K., Strynadka, N. C. & Egelman, E. H. (2006). Structural polymorphism in bacterial EspA filaments revealed by cryo-EM and an improved approach to helical reconstruction. *Structure*, in the press.
28. Rivetti, C., Guthold, M. & Bustamante, C. (1996). Scanning force microscopy of DNA deposited onto mica: equilibration versus kinetic trapping studied by statistical polymer chain analysis. *J. Mol. Biol.* **264**, 919–932.
29. Orlova, A. & Egelman, E. H. (1993). A conformational change in the actin subunit can change the flexibility of the actin filament. *J. Mol. Biol.* **232**, 334–341.
30. Yang, S., Yu, X., Galkin, V. E. & Egelman, E. H. (2003). Issues of resolution and polymorphism in single-particle reconstruction. *J. Struct. Biol.* **144**, 162–171.
31. Galkin, V. E., Orlova, A., Fattoum, A., Walsh, M. P. & Egelman, E. H. (2006). The CH-domain of calponin does not determine the modes of calponin binding to F-actin. *J. Mol. Biol.* **359**, 478–485.
32. Trachtenberg, S., Galkin, V. E. & Egelman, E. H. (2005). Refining the structure of the Halobacterium salinarum flagellar filament using the iterative helical real space reconstruction method: insights into polymorphism. *J. Mol. Biol.* **346**, 665–676.

Edited by W. Baumeister

(Received 10 April 2006; received in revised form 26 May 2006; accepted 12 June 2006)
Available online 30 June 2006